Andrea Belleri, Alessandra Marini, Paolo Riva, Roberto Nascimbene. 2017. "Dissipating and re-centring devices for portal-frame precast structures". Engineering Structures, 150:736-745
DOI: 10.1016/j.engstruct.2017.07.072.

Publisher's version:
http://dx.doi.org/10.1016/j.engstruct.2017.07.072

Dissipating and re-centring devices for portal-frame precast structures

Andrea Belleri[1a], Alessandra Marini[a], Paolo Riva[a], Roberto Nascimbene[b]

[a] Department of Engineering and Applied Sciences, University of Bergamo, Italy
[b] European Centre for Training and Research in Earthquake Engineering, Pavia, Italy

Abstract

The seismic response of buildings not specifically designed to resist earthquake actions can be generally improved by allowing the structure to dissipate an appropriate amount of energy. The use of passive devices for improving the seismic performance of precast concrete structures is investigated herein. In industrial and commercial precast concrete buildings, these devices can be successfully applied at the beam-to-column connections of hinged portal-frames, in order to increase the connection degree of fixity and the dissipated energy during a seismic event. The specific aspects and efficiency of passive dissipation devices based on rotational friction with and without the addition of a re-centring device is analyzed herein. Such devices may be applied both to existing and new buildings; indeed, they are able to mitigate the inter-storey drift demand, to limit the damage at the column base and to reduce residual drifts.
A design procedure is developed in the paper for portal-frames implementing the investigated devices. A case study representing a single-storey precast concrete portal-frame is selected. The design procedure is applied to the case study, considering various devices configurations. The structural performance is assessed by means of non-linear time history analyses.

Keywords:
precast concrete structures; precast connections; re-centring; energy dissipation; beam-to-column joint; portal frame;

[1] Ph.D.; assistant professor, corresponding author, andrea.belleri@unibg.it

1. Introduction

Precast structures are widely recognized as being able to ensure several benefits such as the ability to cover large surfaces, by means of pre-stressed concrete beams, the high quality control of materials and elements, and the reduced construction time compared to traditional reinforced concrete (RC) structures. For the aforementioned reasons, such structures have been commonly adopted in the industrial and commercial sectors, where single-storey or few-storey buildings are characterized by a simple structural layout: cantilever columns pin-connected **[1-3]** to pre-stressed beams supporting pre-stressed roof elements. The columns are placed inside cup footings **[4]** or connected to the foundation by means of mechanical devices or grouted sleeves **[5-7]**. The energy dissipation capacity is generally provided by the development of plastic hinges at the base of the columns.

The beam-to-column connections are usually dry-assembled in place in order to speed up the erection sequence, leading to more flexible structures compared to cast in place RC connections. The building typology being investigated is characterized by a lower displacement ductility demand compared to traditional RC buildings, due to the inherent storey height; indeed, doubling the inter-storey height reduces by half the ductility demand. The lower value of the ductility demand leads to a design focused on controlling the lateral displacement demand rather than limiting the deformation of the materials.

Recent earthquakes in Italy have highlighted the vulnerability of precast structures not designed according to modern seismic codes **[8-11]**. The main vulnerabilities observed are related to inadequate horizontal load transfer mechanisms between precast members leading to the loss of support and consequent fall of both structural **[11-14]** and non-structural elements, as for instance cladding panels **[15-17]**. Additional loads in existing connections arise as a consequence of displacement incompatibility between adjacent elements due to the high flexibility of the considered structures. Such load increase could happen in the connections between beams and columns **[18]**, between roof elements and supporting beams **[19]** and between cladding panels and supporting elements **[15]**.

This paper focuses on the reduction of seismic lateral displacements and seismic damage in hinged portal-frames by providing beam-to-column connections, suitable for both new and existing buildings. This task can be achieved either with connections in emulation of cast-in-place RC structures **[20-22]** or with additional mechanical devices at the beam-to-column joint. The former solution involves formworks and additional castings with consequent increase of the erection time for new structures and operational difficulties in the case of existing buildings. The latter solution is fully compatible with the traditional construction sequence, indeed the additional devices are put in place at the end of the erection sequence. Consequently the solution is suitable also for existing buildings. The beam-to-column devices provide a source of additional damping to the system (i.e. dissipation of seismic energy) and a degree of fixity to the beam-to-column joint (i.e. increase of lateral stiffness).

Starting from solutions available in the literature **[23, 24]**, the paper investigates the most suitable arrangements for beam-to-column additional devices in order to be fully compatible with the seismic deformations arising in portal-frame structures. A design procedure is proposed and the suitability of the investigated devices is validated by means of non-linear time history analyses on a selected case study resembling a portal-frame of a precast industrial building. The paper considers the performance in the transverse direction of portal-frame structures; however, it is possible that additional devices could be applied in the longitudinal direction, for example between columns and gutter beams or between adjacent precast cladding panels **[25]**.

2. Beam-to-column connection devices

In order to select the most suitable additional devices for beam-to-column joints of new and existing precast concrete structures, the following properties should be considered:

1. compatibility between the device and the considered hinged portal-frame static scheme;
2. assembling by means of dry post-installed connections;

3. avoid interference with floor activities, for instance by placing the devices at the side or underneath the main girders;
4. stable dissipation capacity;
5. easy substitution after an earthquake;
6. limited damage in the beams and in the columns as a consequence of the device installation, with the exception of plastic hinge formation at the base of the columns;
7. re-centring capacity if available.

Two devices are selected herein in accordance to the aforementioned properties. Such devices have different characteristics and they can be applied as single devices or as devices acting in parallel.

The first device, whose potential was previously investigated both analytically and through numerical analyses **[24]**, is able to dissipate energy through the friction generated by the relative rotation of steel plates with interposed brass discs. The interposition of brass discs, softer than the connected steel plates, is necessary to guarantee smoothness during relative rotations. The energy dissipation increases the system damping and it is therefore beneficial especially in the case of seismic events which do not present "near field” characteristics, i.e. conditions in which the maximum deflection of the system is reached before fully engaging its dissipative capacity. Indeed, the maximum efficiency of a dissipation device is associated to a steady-state response, as evidenced by the concept of equivalent viscous damping **[26]**.

Ideally, the adopted devices should be able to both dissipate energy and provide an appropriate degree of fixity at the beam-to-column joint in order to increase the system lateral stiffness. This could be accomplished by introducing a second elastic device able to limit the residual deformations as it is shown in the following. The two selected devices can be coupled and calibrated to dissipate a sufficient amount of energy, and to allow re-centring of the connection after an earthquake.

The optimal position of the devices, graphically represented in **Figure 1a,** is selected to maximize their performance under a seismic event. A kinematic analysis has been carried out to check the compatibility between the investigated devices and the considered hinged portal-frame structural system. The position of the friction-rotation dissipation devices, shaded circles in **Figure 1a**, is selected to obtain an articulated quadrilateral with the beam-to-column joint (hinges 1-4 in **Figure 1a**) once the static friction load is overcome. This configuration does not significantly increase the lateral stiffness of the system. The position of the stiffening/re-centring device is selected to create a statically determinate triangle within the beam and column ends. This configuration is characterized by a high stiffening effect. It is worth noting that the proposed solution requires a mechanical connection at the beam-to-column joint. In buildings designed according to modern seismic codes, this connection is actually provided to transfer seismic actions among structural elements. In older buildings, as in the case of the precast industrial buildings damaged by the 2012 Emilia earthquake **[8-11]**, horizontal loads may be transferred by friction. In such conditions, additional mechanical connections are required as retrofit measure to transfer seismic loads and to avoid out-of-plane failure of the reinforced concrete fork **[11]**, even without the application of the additional devices investigated herein. U-shape steel profiles at the column sides may accomplish to this task (**Figure 1a**). It is observed that the stiffening device could be substituted by friction-linear or other hysteretic systems to provide both energy dissipation and the stiffening of the beam-to-column joint. Finally, it is worth noting that the investigated devices can be substituted by proprietary devices if available.

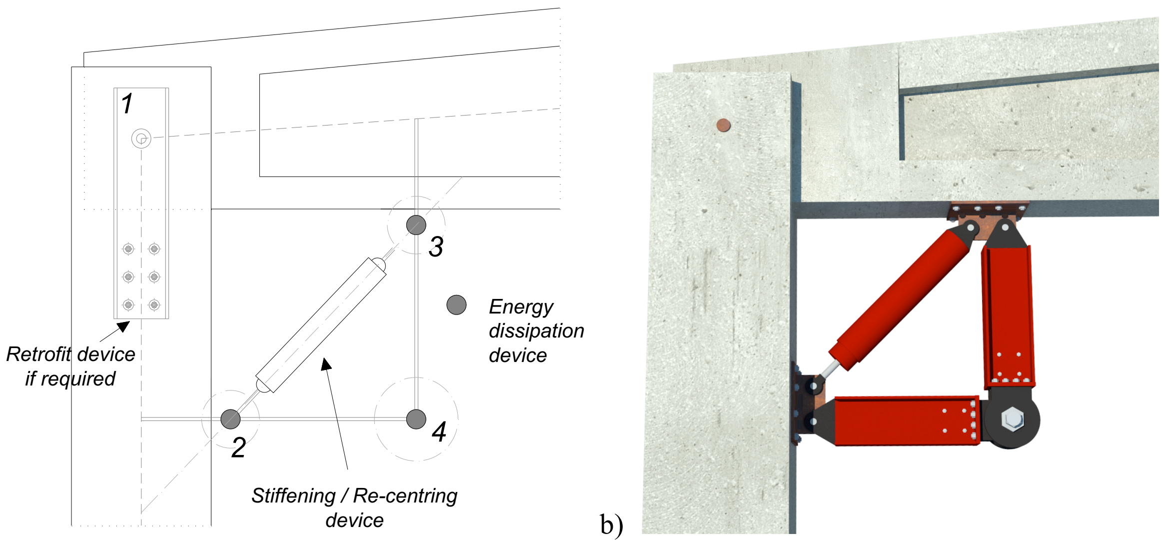

a) b)

Figure 1 – a) Beam-to-column devices optimal position with a retrofit device if required for existing buildings; b) example of coupled devices.

2.1 Energy dissipation (ED) device

The energy dissipation (ED) device considered herein can be applied in correspondence of the three hinges depicted in **Figure 1a**. Such device dissipates energy through friction due to the relative rotation of its elements. In the present study, the application of sliding surfaces only at the bottom-right hinge of **Figure 1a** is considered, the remaining hinges are free to rotate. The performance of the device is optimized by the insertion of brass discs as shown in **Figure 2**. Other materials can be adopted. Brass discs are softer than the connected steel plates. This guarantees smoothness during relative rotations. In addition a small difference between static and dynamic coefficient of friction is observed, respectively 0.51 and 0.44 **[27]**, which allows for stable and uniform hysteretic response.

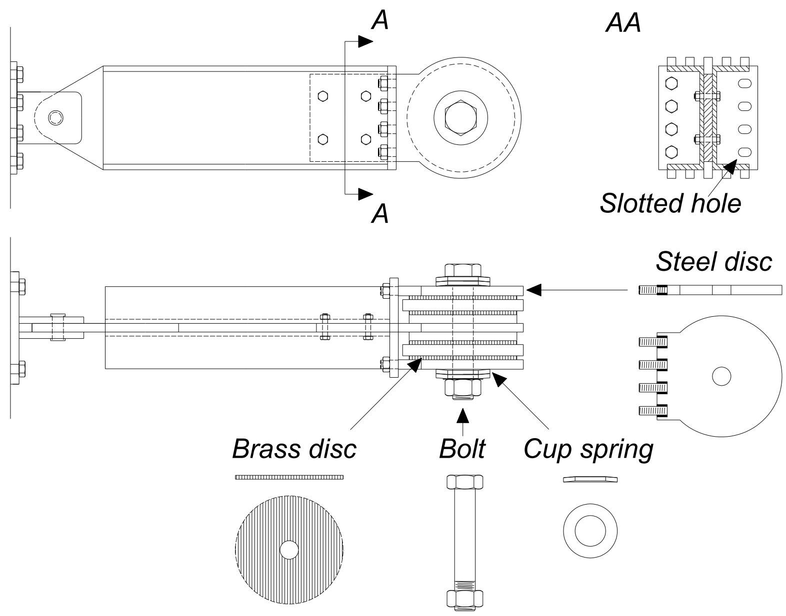

Figure 2 – Friction-rotation dissipative device

Figure 2 shows a possible solution to increase the system energy dissipation by increasing the device activation moment. This is accomplished by incrementing the number of sliding surfaces. The steel discs are fixed to the mounting frame by bolts placed in slotted holes. This detail is required to allow the whole transferring of the external tightening force to the brass discs; indeed eventual transverse displacements of the steel discs due to the tightening force are accommodated by the slotted holes. The setup shown in **Figure 2** allows for 4 sliding planes. Cup springs are provided on the main bolt for a better control of the tightening load acting on the brass discs.

The bending moment associated to the sliding of the brass surfaces in dynamic conditions is:

$$M = \int_{\rho=R_i}^{R_e} \int_{\theta=0}^{2\pi} \rho^2 \cdot \mu \cdot \frac{N}{\pi\left(R_e^2 - R_i^2\right)} \cdot d\rho d\theta = \frac{2}{3}\mu \cdot N \cdot \frac{R_e^3 - R_i^3}{R_e^2 - R_i^2} \tag{1}$$

where μ is the dynamic coefficient of friction, N is the bolt pre-tension load and R_e, R_i are the external radius and internal radius of the brass disc respectively, ρ and θ are integration variables in the polar coordinate system. **Table 1** shows the activation friction moment of the device for selected configurations and in dynamic conditions, i.e. considering the dynamic coefficient of friction.

Table 1 – Dynamic friction activation moment of the ED device.

Bolt diameter (mm)	Bolt class **[28]**	Bolt pre-tension (kN)	Activation moment (kNm)
2 sliding surfaces – R_e = 125 mm; R_i = 25 mm			
39	8.8	440	33
39	10.9	550	41
48	8.8	650	50
48	10.9	820	62
4 sliding surfaces – R_e = 125 mm; R_i = 25 mm			
39	10.9	550	82
48	8.8	650	100
48	10.9	820	124
8 sliding surfaces – R_e = 125 mm; R_i = 25 mm			
39	10.9	550	164
48	8.8	650	200
48	10.9	820	248

Taking as reference a portal frame with the additional ED device (**Figure 3**), it is possible to evaluate the internal actions and the lateral stiffness of the resulting system. An inflection point at the beam midspan is considered. The internal actions, obtained from equilibrium, are expressed in terms of the seismic load acting on the half frame (F/2):

$$V_A = \frac{F}{2}; \quad N_A = V_E = \left(\frac{F}{2} \cdot H - M_A\right) \cdot \frac{2}{L}; \quad f = \left(\frac{F}{2} \cdot H - M_A\right) \cdot \frac{1}{b} \tag{2; 3; 4}$$

The bending moment at the column base and the system lateral stiffness are obtained applying the principle of virtual works on the half frame represented in **Figure 3**:

$$M_A = \frac{F}{2} H \frac{\left(\frac{4}{EI_2} + \frac{L}{EI_1 H}\right) + \frac{4L}{b}\left(\frac{1}{EI_3} - \frac{1}{EI_2} - \frac{1}{EI_1}\right) + \frac{L}{b^2}\left(\frac{3H}{EI_1} + \frac{L}{EI_2}\right)}{\frac{4}{EI_2} + \frac{4L}{b}\left(\frac{1}{EI_3} - \frac{1}{EI_2} - \frac{1}{EI_1}\right) + \frac{L}{b^2}\left(\frac{6H}{EI_1} + \frac{L}{EI_2}\right)} \tag{5}$$

$$k = \frac{3EI_1}{H^3} \frac{\frac{16}{EI_2} + \frac{16L}{b}\left(\frac{1}{EI_3} - \frac{1}{EI_1} - \frac{1}{EI_2}\right) + \frac{4L}{b^2}\left(\frac{6H}{EI_1} + \frac{L}{EI_2}\right)}{2\left(\frac{4}{EI_2} + \frac{3L}{EI_1 H}\right) + \frac{8L}{b}\left(\frac{1}{EI_3} - \frac{1}{EI_1} - \frac{1}{EI_2}\right) + \frac{L}{b^2}\left(\frac{3H}{EI_1} + \frac{2L}{EI_2}\right) - \frac{b^2 L}{EI_1 H^3}} \tag{6}$$

where EI_1, EI_2, EI_3 are the flexural stiffness of the column, beam and energy dissipation device, respectively. E is the elastic modulus and I is the second moment of area of the considered cross-section.

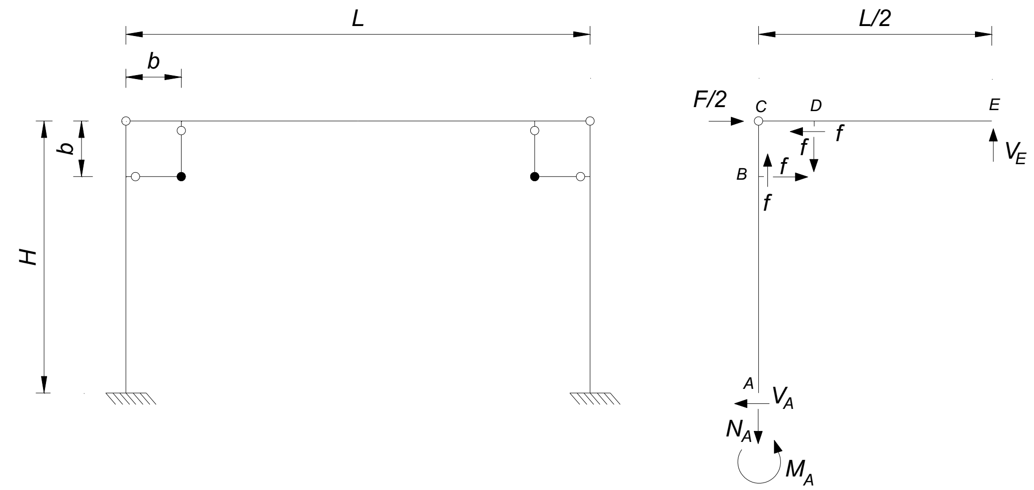

a) b)

Figure 3 – a) Portal frame with the additional ED devices; b) considered static scheme.

2.2 Stiffening and Re-centring (SR) device

The stiffening and re-centring (SR) device provides a degree of fixity at the beam-to-column joint and minimizes the residual deformations after a seismic event. In this paper, the use of a device adopting cup springs is explored, although other solutions can be adopted, such as ring springs or shape memory alloys. The peculiarity of the device being investigated is its ability to exploit the compressive behaviour of the springs for actions that tend both to shorten and lengthen the device itself. As depicted in **Figure 4**, the internal springs undergo a compression when the device is subject either to compression or tension.

It is possible to use cup springs with or without initial pre-compression. In the first case the device acts as a rigid system until the pre-compression of the springs is overcome; while in the second case the device acts as a spring depending on the number and arrangement of cup spring stacks. The available stroke is governed by the number of spring stacks in series, while the number of springs in parallel governs the resistance. In the case of pre-stressed springs, the available stroke is obtained subtracting the displacement already assigned to pre-compress the springs. It is important to provide adequate displacement capacity to the device, in order to avoid full packing of the springs. Herein, the 90% of the available stroke of the springs is considered to sustain 2.5% of lateral drift of the system. **Table 2** shows the characteristics of the SR device for selected configurations. It is essential to note that the available stroke influences the device performance. Indeed, the maximum stroke of the device should be determined referring to a high intensity earthquake (2% probability of exceedance in 50 years). In the case of pre-compression, the device activation load is determined referring to the design basis earthquake (10% probability of exceedance in 50 years).

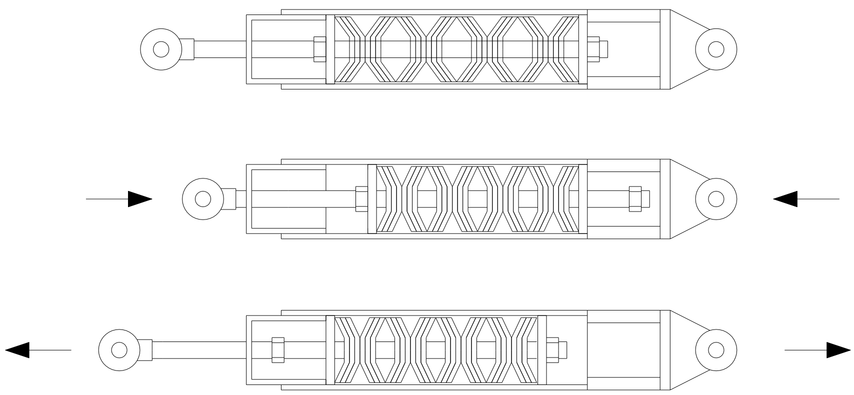

Figure 4 – Scheme of the SR device.
Note: the depicted devices includes 8 stacks of cup springs, with 3 springs each.

Taking as reference the same half portal-frame shown in **Figure 3**, it is possible to evaluate the internal actions (**Eq.2-4**) and the lateral stiffness of the resulting system:

$$M_A = \frac{F}{2} H \frac{\frac{12}{k_{dis} b} + \frac{b^2}{EI_1 H} - \frac{4b}{EI_1} + \frac{3H}{EI_1} - \frac{4b}{EI_2} + \frac{4b^2}{EI_2 L} + \frac{L}{EI_2}}{\frac{12}{k_{dis} b} - \frac{4b}{EI_1} + \frac{6H}{EI_1} - \frac{4b}{EI_2} + \frac{4b^2}{EI_2 L} + \frac{L}{EI_2}} \tag{7}$$

$$k = \frac{3EI_1}{H^3} \frac{\frac{48L}{b^4 k_{dis}} + \frac{24LH}{b^2 EI_1} + \frac{4L^2}{b^2 EI_2} - \frac{16L}{b} \frac{EI_1 + EI_2}{EI_1 EI_2} + \frac{16}{EI_2}}{\frac{24L}{b^4 k_{dis}} + \frac{3HL}{b^2 EI_1} + \frac{2L^2}{b^2 EI_2} - \frac{8L}{b} \frac{EI_1 + EI_2}{EI_1 EI_2} + \frac{8}{EI_2} + \frac{6L}{EI_1 H} - \frac{b^2 L}{EI_1 H^3}} \tag{8}$$

where k_{dis} is the axial stiffness of the SR device.

It is worth mentioning that the previous formulation could be adopted also for linear dissipation devices, such as linear friction or hysteretic systems, as the INERD pin connection **[29]**.

Table 2 – Characteristics of the SR device (device length 1.41m).
Note: d_e cup spring external diameter; d_i cup spring internal diameter;
t cup spring thickness; k_{dis} device stiffness after pre-compression; N is the design axial load and the pre-compression load for SR devices with and without pre-compression respectively.

d_e (mm)	d_i (mm)	t (mm)	n° springs per stack	n° stacks	N (kN)	k_{dis} (kN/mm)
Without pre-compression						
50	25.4	3	5	14	70	4.7
50	25.4	3	10	14	125	9.5
80	36	4	10	7	250	15.1
80	41	5	13	9	500	35.3
With pre-compression						
100	41	4	5	9	70	4.1
100	41	4	9	9	125	7.4
125	51	5	11	8	250	12.3
150	61	6	17	6	500	33.1

2.3 Coupling ED and SR devices

The coupling of the two devices may bring significant benefits to the system, reducing the seismic demand in terms of both lateral displacements and residual deformations. The moment-rotation relationship of the connection may assume a flag shape hysteresis loop (**Figure 5**), leading to full re-centring of the beam-to-column joint. The use of the investigated additional devices leads to a gradual increase of the system lateral stiffness as indicated in **Figure 6**, which shows the ratio between the lateral stiffness of a system implementing different devices and the lateral stiffness of a hinged portal-frame. The system with only ED devices has a behaviour and stiffness comparable to a hinged portal-frame, with a small increase of the load demand at the beam-to-column joint. The addition of dissipative devices is therefore suitable as a retrofit solution for existing buildings, without significant retrofit and strengthening measures at the beam and column ends. The use of SR devices leads to a structural stiffness similar to a portal-frame with rigid connections, with a load distribution at the beam and column ends completely different from that of a hinged portal-frame. The addition of SR devices is therefore more appropriate in the case of new buildings rather than for the retrofitting of existing structures. However, it is possible to use such devices also in existing buildings provided that strengthening measures are undertaken for the beam-to-column joint to withstand the increased load demand.

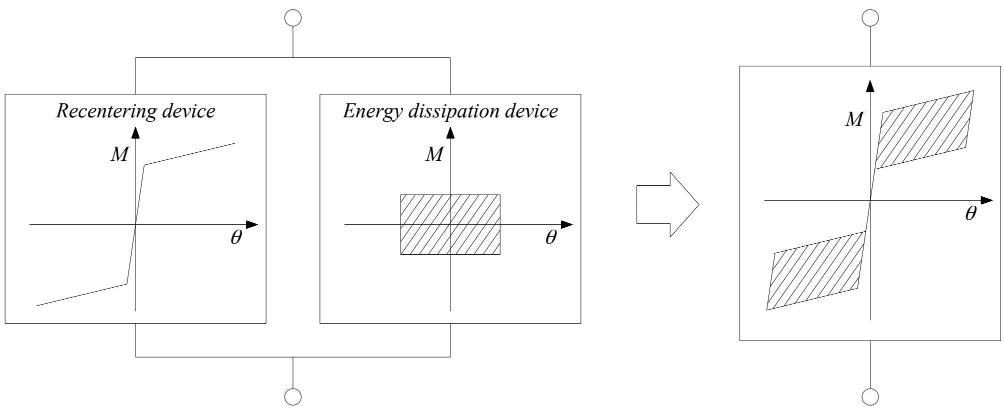

Figure 5 – Coupling of ED and SR devices.

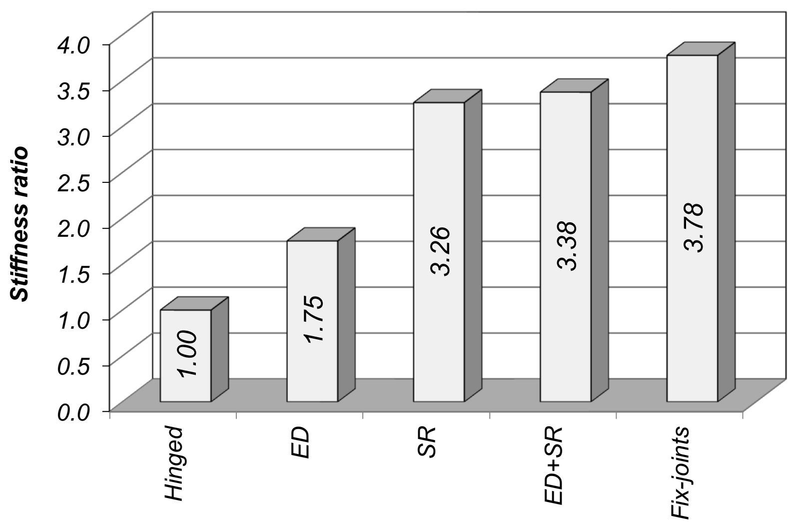

Figure 6 – Stiffness ratio between hinged portal-frame with and without additional devices.

As in the case of single devices, it is still possible to determine the bending moment at the column base and the system lateral stiffness by applying the principle of virtual works:

$$M_A = \frac{F}{2} H \frac{\frac{12}{k_{dis} b} + \frac{b^3}{EI_1 H} - \frac{4b^2}{EI_1} + \frac{3Hb}{EI_1} - \frac{4b^2}{EI_2} + \frac{4b^3}{EI_2 L} + \frac{Lb}{EI_2} - \frac{24\alpha}{k_{dis} b} + \frac{12\alpha^2}{k_{dis} b} + \frac{4b^2\alpha^2}{EI_3}}{\frac{12}{k_{dis} b} - \frac{4b^2}{EI_1} + \frac{6Hb}{EI_1} - \frac{4b^2}{EI_2} + \frac{4b^3}{EI_2 L} + \frac{Lb}{EI_2} - \frac{24\alpha}{k_{dis} b} + \frac{12\alpha^2}{k_{dis} b} + \frac{4b^2\alpha^2}{EI_3}} \tag{9}$$

$$k = \frac{\frac{3EI_1}{H^3}\left[\frac{16}{EI_2} + \frac{4L}{b^2}\left(\frac{6H}{EI_1} + \frac{L}{EI_2}\right) + \frac{48L}{b^4 k_{dis}}\left(-1+\alpha\right)^2 + \frac{16L}{b}\left(\frac{\alpha^2}{EI_3} - \frac{EI_1 + EI_2}{EI_1 EI_2}\right)\right]}{\frac{8}{EI_2} + \frac{2L}{b^2}\left(\frac{6H}{EI_1} + \frac{L}{EI_2}\right) + \frac{24L}{b^4 k_{dis}}\left(-1+\alpha\right)^2 + \frac{8L}{b}\left(\frac{\alpha^2}{EI_3} - \frac{EI_1 + EI_2}{EI_1 EI_2}\right) - \frac{L}{EI_1 H}\left(\frac{b}{H} - \frac{3H}{b}\right)^2} \tag{10}$$

The coefficient α is the portion of load f (**Figure 3**) transferred to the ED device as in **Figure 7**:

$$\alpha = \frac{3EI_3}{k_{dis} b^3 + 3EI_3} \tag{11}$$

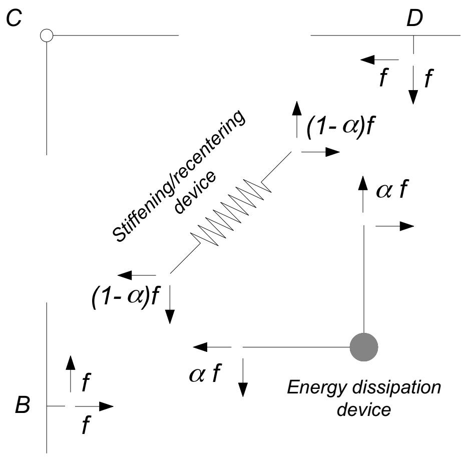

Figure 7 – Load distribution in the case of coupled devices.

3. Performance of the additional devices

A case study is selected to evaluate the performance of the investigated devices. A portal-frame resembling an existing precast industrial building is considered (**Figure 8**); the tributary roof mass (m_{roof}) is 110,000 kg. The building is located in L'Aquila (Italy) and the spectral shape is derived according to the Italian building code **[30]**. An importance factor **[30]** equal to 2 is considered to account for industrial buildings dealing with environment-dangerous activities. As a result, the return period associated to the life safety limit state is 949 years. In addition, the site rests on a slope with an angle greater than 15°, which leads to a topographic amplification factor **[30]** equal to 1.2. The resulting spectral shape is compatible with EN 1998-1 **[31]** type 1 spectrum with soil class C and with peak ground acceleration (PGA) equal to 0.54 g. The serviceability limit state is characterized by a *PGA* equal to 0.22 g. Two sets of non-linear time history analyses are conducted on the selected frame considering different sources of ground excitation. The first set of analyses is carried out to derive general considerations on the devices; an artificial spectrum-compatible record generated with the SIMQKE-1 algorithm **[32]** is used. The second set of analyses is carried out to validate the design procedure that is presented in the following; in this case the ground excitation is provided by a set of 7 ground motions[2], selected and scaled from the European strong motion database **[33]** in order to be spectrum compatible. 30 s of zero acceleration are added at the end of each ground motion to capture residual roof displacements. All the analyses are carried out with the software MidasGen **[34]** considering 3% Rayleigh for the periods 0.3 s and 1.0 s.

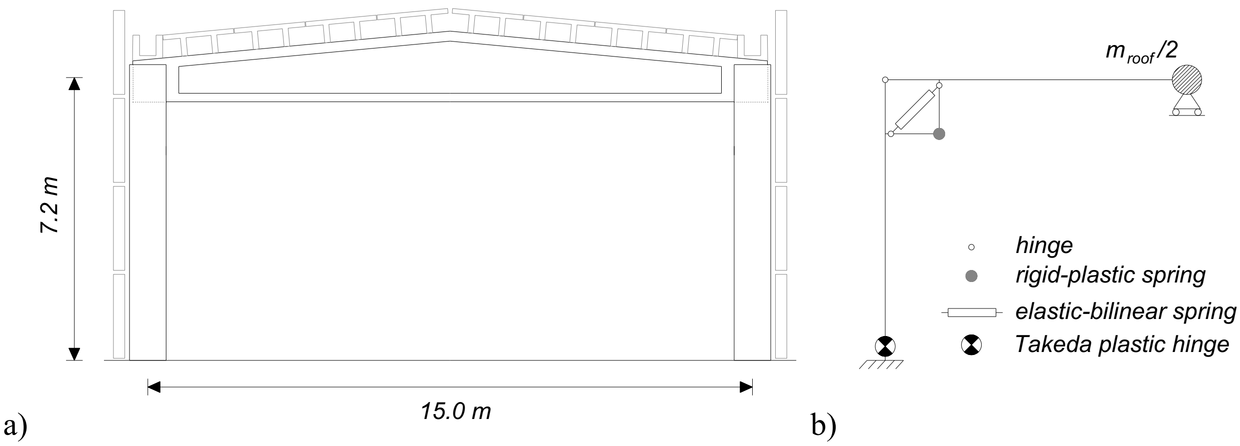

Figure 8 – a) Considered case study; b) scheme of the finite element model.

3.1 General performance evaluation

In the first set of analyses, a square (70x70 cm) column cross-section is selected. The longitudinal reinforcement is provided by twenty-four 20 mm diameter rebars (steel percentage 1.54%). The lever arm of the additional devices (**Figure 3**) is b = 1 m. The ED device is made by 2 UPN 240 steel profiles; the ED activation moment is selected as a portion of the column base bending

[2] Record code [32] and adopted scale factor (in brackets): 000198ya (2.38), 000413xa (2.48), 001257ya (2.18), 000333xa (2.32), 000291ya (3.03), 001703ya (1.04), 000879xa (2.36)

moment capacity. The SR device, 1.41 m long, is made by a steel pipe with external diameter 176 mm and thickness 8 mm; the spring pre-compression varies to evaluate its influence on the structural response.

Considering the finite element model scheme in **Figure 8**, the plastic hinge at the column base is modelled with Takeda hysteresis **[35]**. A tri-linear model is adopted with moment at yield and at maximum capacity equal respectively to 955 kNm and 1142 kNm. According to Takeda cyclic behaviour, the unloading stiffness is equal to a fraction of the elastic stiffness to account for stiffness degradation after yielding. Such reduction factor is equal to the ratio, raised to the power of 0.35, between the yield displacement and maximum displacement. The reloading branch targets a point on the skeleton curve corresponding to the maximum inelastic deformation reached in the loading direction. A plot of the cyclic behaviour of the plastic hinge at the column base is shown in the following. The horizontal girder is modelled as an elastic beam element. Assuming the inflection point due to seismic loading at the girder midspan, only half of the girder is considered and a horizontal roller is placed at the beam end. The arms of the ED device are modelled as elastic beam elements while the hysteresis due to friction is provided by a rigid-plastic rotational spring. The SR device is modelled as an elastic-bilinear spring.

To evaluate the influence of the devices, the parameter β is introduced. β is the ratio between M_0 and $M_{0\,el}$. M_0 is the device activation moment which has been actually provided. $M_{0\,el}$ is the device activation moment which leads to the simultaneous activation of the device (i.e. $M_{0\,el}$) and yielding at the column base (M_y). In the case of ED devices, M_0 is the friction activation moment; in the case of SR device, M_0 is defined as the pre-compression load (N_0) times b/√2. $\beta = 0$ corresponds to the bare frame response; indeed the activation moment of the device is so low that makes the device ineffective. $\beta = 1$ corresponds to the simultaneous activation of the device and yielding at the column base. $M_{0\,el}$ is obtained following the previous analytical derivation. Given the yield moment at column base (M_y), the lateral force F associated to its development is obtained substituting M_y to

M_A in **Eq. 5, 7, 9** for the ED device, SR device and coupled devices respectively; f (**Figure 3**) is obtained from **Eq. 4**, which allows determining $M_{0\,el}$.

Figure 9 shows the results of non-linear time history analyses for the aforementioned spectrum-compatible record. The results are expressed as a function of β in terms of roof lateral displacement, base shear, energy dissipation at the column base and load at the beam-to-column connection. Considering the roof displacements, the ED case presents a gradual reduction as the energy dissipation increases, the SR case is characterised by almost constant displacements, while the ED+SR case shows a minimum value for β=60%. Concerning the base shear, a monotonic increase is observed for all the cases. Higher values are recorded for the SR and ED+SR cases compared to the ED case. This is a consequence of the high stiffness of the beam-to-column joint associated with the re-centring device. Looking at the load arising in the beam-to-column connection, the ED case is characterised by values lower than the hinged portal-frame. The joint stiffening effect due to re-centring devices leads to significant joint loads, up to 5 times the load obtained in the bare frame case. Finally, as regards the energy dissipation at the column base, i.e. the eventual damage, the maximum reduction is obtained in the case of coupled devices.

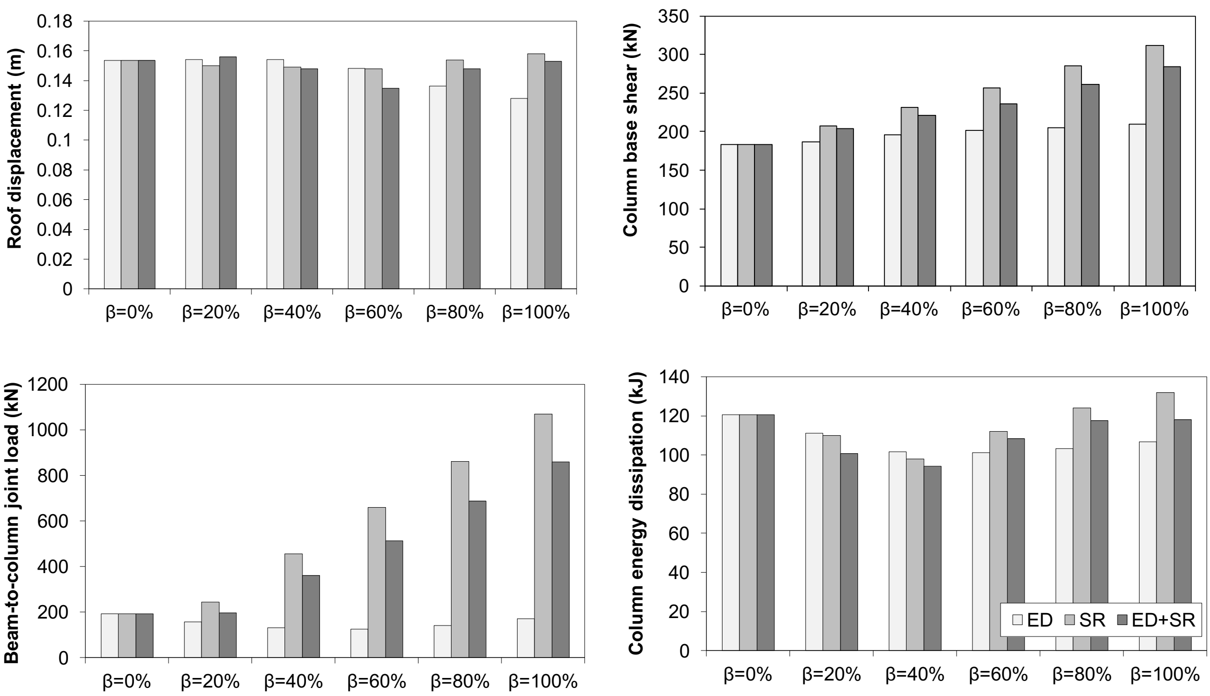

Figure 9 – Influence of ED, SR and ED+SR devices.

3.2 Definition and validation of a design procedure

A simplified design procedure is herein proposed in accordance to linear static methodologies found in national and international building codes **[30, 31, 36]**, usually referred to as "force based design procedures". In the first step of the considered design procedure, the cross-section of the column is estimated considering a target lateral displacement (Δ_{sls}) at the serviceability limit state (SLS). Because the period of vibration of the considered structural typology typically lays in the constant velocity region of the pseudo-acceleration spectrum, the column base B (square cross-section) is obtained equating the force associated with the spectral acceleration and the force related to the target displacement:

$$\begin{cases} F = m \cdot S(T) = m \cdot 2.5 \cdot PGA \cdot \dfrac{T_c}{T} = \dfrac{m \cdot 2.5 \cdot PGA \cdot T_c}{2\pi\sqrt{m/k}} \\ F = k \cdot \Delta = \chi \dfrac{EI_1}{H^3} \cdot \Delta = \chi \dfrac{E \cdot B^4}{12 \cdot H^3} \cdot \Delta \end{cases} \Rightarrow B = \sqrt{\frac{2.5 \cdot PGA \cdot T_c}{2\pi \cdot \Delta} \sqrt{\frac{6 \cdot m \cdot H^3}{\chi \cdot E}}} \quad (12)$$

where *PGA* is the peak ground acceleration at SLS, *S(T)* is the spectral acceleration value at period *T*, *k* is the lateral stiffness, *m* is the roof tributary mass. χ is a coefficient accounting for the system stiffness in the case of ED or SR devices; in particular χ is taken equal to 3 for ED devices, i.e. assuming columns as cantilevers, and equal to 12 for SR and ED+SR devices, i.e. assuming columns in double bending. It is worth mentioning that the obtained value of *B* is a first estimation and, if required, it will be modified.

In the second step, a first estimate of the geometry of the additional devices is determined, as, for instance, resulting from geometry compatibility, aesthetic issues or due to the availability of proprietary devices in the market. Only the geometry of the device is defined at this stage, while the ED activation moment and the SR pre-stress are defined in another step. The system lateral stiffness is therefore determined from **Eq. 6, 8 and 10** based on the considered devices. This allows determining the fundamental period of vibration of the system, $T=2\pi\sqrt{(m/k)}$, and the seismic load corresponding to the design basis earthquake (DBE), $F_{DBE} = m \cdot S(T)$. A behaviour factor (q) equal to 2 is herein adopted, owing to the flexibility of the considered structural system. S(T) is the design spectral acceleration including the behaviour factor. Given F_{DBE}, the associated yield moment at the column base is obtained from **Eq. 5, 7 and 9** based on the adopted devices. The load acting on the device is obtained from **Eq. 4 and 11**. The obtained activation load of the device is reduced by a factor β to assure the activation of the device before column yielding. β is taken equal to 60-70% for ED and 40-50% for SR or ED+SR devices consequently to the results of the previous chapter. Iterations are required if either the device or the column do not sustain the seismic load.

The design procedure is applied to the selected case study and the results are reported in **Table 3** for different configurations of the additional devices. It is observed that the ED case is characterised by wider dimensions of the column cross-section and by a higher amount of rebars compared to the SR or ED+SR cases.

Table 3 – Procedure results for the selected case study.
Note: k is the portal stiffness; $M_{u\,dp}$ is the base moment obtained from the design procedure; $M_{u\,prov}$ is the base moment actually provided; M_y is the base moment at yield; M_{ED} is ED activation moment; F_{SR} is SR pre-compression load.

	ED	SR	ED + SR	Bare $_{ED}$
k (kN/m)	9,252	11,144	11,652	7,464
$M_{u\,dp}$ (kNm)	1,999	860	864	-
Cross section (m x m)	0.75 x 0.75	0.65 x 0.65	0.65 x 0.65	0.75 x 0.75
Re-bars number-diameter (mm)	28–24	24–22	24–22	28–24
$M_{u\,prov}$ (kNm)	2,035	1,286	1,286	2,035
M_y (kNm)	1,433	925	925	1,433
β	0.65	0.45	0.55	-
M_{ED} (kNm)	145	-	60	-
F_{SR} (kN)	-	475	530	-

Non-linear time history analyses are conducted considering the same finite element model scheme depicted in **Figure 8** and the same type of elements previously outlined. The aforementioned set of 7 spectrum-compatible ground motions taken from the European strong motion database is adopted. Both DBE and SLS are analysed. In the latter case, the ground motions have been further scaled by the factor 0.4. An additional model has been investigated, Bare $_{ED}$, considering the same column of the ED case without the energy dissipation device.

The results are reported in **Table 4** as average values ± one standard deviation; the maximum values obtained for each ground motion are considered. An overall good performance of the investigated devices is obtained, highlighting the suitability of the proposed design procedure. In particular, it is observed how the SR case is characterized by the highest roof displacements; this is associated with the higher lateral stiffness, and therefore higher spectral values, and to the lower energy dissipation compared to the other solutions. As expected, both SR and ED+SR cases are characterised by negligible residual roof displacements, owing to the re-centring capability of pre-compressed springs in the SR devices. It is worth noting that the load in the beam-to-column dowel connection is 8%, 69% and 104% higher than the Bare $_{ED}$ case for the ED, SR and ED+SR case respectively.

The shear and bending moment distribution in the column and in the beam are expected to change due to the presence of the additional devices. **Table 4** reports the shear and bending moment in correspondence to the device connection, both in the beam and in the column. The results show that at the device-to-column connection the bending moment and the shear are similar to those of the bare frame. Regarding the device-to-beam connection, the girder of the bare frame is not subjected to bending due to seismic loading as a consequence of the hinged portal-frame static scheme. Therefore the additional bending moment and shear due to the device need to be compared to the corresponding design values (868 kNm and 930 kN, respectively). Considering existing buildings, retrofit measures are required in the case the demand exceeds the capacity. Such interventions can be for instance steel jacketing or fibre reinforced polymer retrofitting. Similarly, the beam-to-column hinge can be strengthened by providing a higher capacity dowel connected to U-shape steel profiles at the column sides [**11**] (**Figure 1a**).

Table 4 – Non-linear time history analyses results.

Note: Δ_{SLS} roof displacement (SLS); Δ_u and Δ_{res} displacement and residual displacement at roof (DBE); F_{conn} force in the connection (DBE); V_b base shear (DBE); $M_{dev\ col}$, $V_{dev\ col}$, column bending moment and shear in correspondence to the device connection (DBE); $M_{dev\ beam}$, $V_{dev\ beam}$, beam bending moment and shear in the in correspondence to the device connection (DBE).

	ED	SR	ED + SR	Bare $_{ED}$
Δ_u (m)	0.166±0.016	0.203±0.030	0.187±0.025	0.193±0.024
Δ_{res} (m)	0.020±0.014	0.004±0.004	0.003±0.004	0.029±0.013
Δ_{SLS} (m)	0.073±0.009	0.075±0.015	0.075±0.015	0.086±0.015
F_{conn} (kN)	221.2±3.0	471.1±8.5	569.9±7.1	279.2±2.3
V_b (kN)	308.6±1.8	232.9±1.0	246.4±0.9	285.3±0.2
$M_{dev\ col}$ *(kNm)*	151.7±3.7	307.2±13.3	327.8±6.1	316.7±4.1
$V_{dev\ col}$ *(kN)*	308.6±1.8	307.2±13.3	327.8±6.1	285.3±0.2
$M_{dev\ beam}$ *(kNm)*	175.5±3.7	356.4±3.4	402.1±3.2	0
$V_{dev\ beam}$ *(kN)*	175.5±3.7	356.4±3.4	402.1±3.2	0

Figure 10 shows an example of hysteretic plots for the case of coupled devices. The plots refer to a single ground motion (ground motion 000198ya according to **[33]**). The comparison is carried out considering a hinged portal-frame (Bare $_{SR}$) with the same column cross section and rebars as in the ED+SR case. It is observed how the additional devices lead to lower rotation demand of the column base **(Figure 10a)** and to lower roof displacement **(Figure 10b)** compared to the bare case. The base shear demand **(Figure 10b)** is higher than the hinged portal-frame solution as a result of the stiffness increase at the beam-to-column joint. **Figure 10c** highlights the flag shape hysteresis resulting from the coupled devices.

It is worth noting that the proposed design procedure, as in general "forced based design" procedures, is not able to account for roof displacement as initial performance target. Being the considered structural typology more flexible compared to traditional reinforced concrete structures due to the adopted static scheme and to the high inter-storey height, the design is generally governed by the control of displacements rather than the control of material strains. Therefore a more rational design approach should consider the lateral displacements as input of the design procedure. Such an approach is represented by the “displacement based design” procedure **[37-39]** whose application on the considered structural typology is a topic of ongoing research.

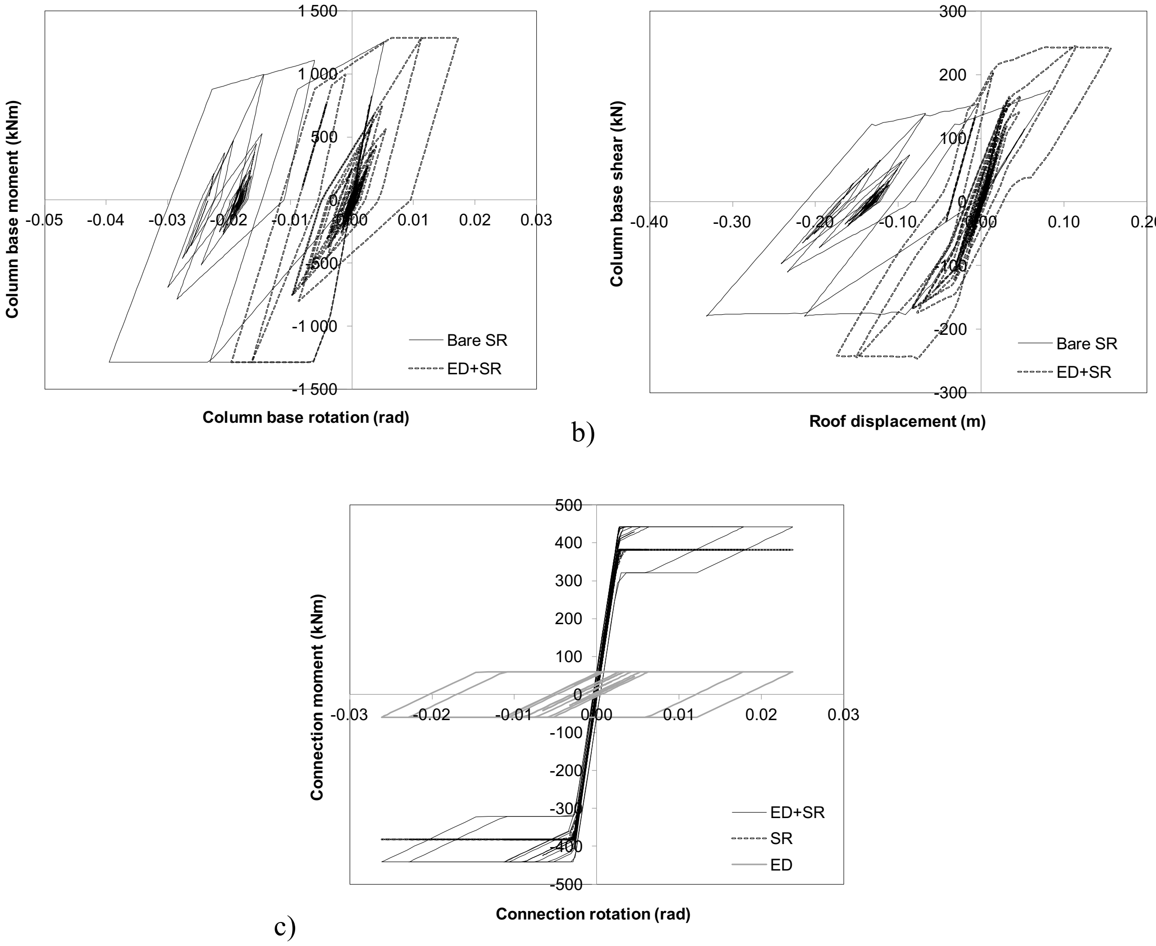

a) b)

c)

Figure 10 – Example of time history plots for the ED+SR case (ground motion 000198ya according to **[33]**):
a) column base moment-rotation with and without devices;
b) base shear-roof displacement with and without devices;
c) moment-rotation components of the beam-to-column connection.
Note: Bare SR refers to a hinged frame with the same column cross section and rebars as in the ED+SR case

Conclusions

The paper investigates the performance of two mechanical devices to be applied at the beam-to-column joint of typical precast hinged portal-frames to dissipate seismic energy and to reduce lateral displacements, column damage and residual deformations. Such devices, being installed after completing the erection phase, are compatible with pre-stressed elements and with the construction practice of typical precast industrial buildings. The devices are not activated by gravity dead load but only by additional loads such as earthquakes. Indeed, in a first phase the pre-stressed beams act as simply supported elements, subjected to gravity loads; in a second phase, as in the case of seismic events, the devices provide a degree of restraint at the beam-to-column joint.

The first device, namely the energy dissipation (ED) device, provides energy dissipation through friction by relative rotation of steel and brass discs: the hysteretic damping of the system increases with a consequent reduction of the load demand in the structural elements. The second device, namely the stiffening/re-centring (SR) device, increases the stiffness of the beam-to-column joint and reduces the residual deformations of the system; the use of pre-tension provides a bilinear elastic load-displacement relationship. The two devices could be used in parallel. The friction activation moment of ED devices and the pre-tension of SR devices can be selected in order to lead to a flag-shape hysteresis of the coupled system. The use of the devices leads to a gradual increase of the system stiffness, due to a gradual shift of the beam-to-column joint from a pin to a fixed connection. During an earthquake, the use of the devices provides a general reduction of the column damage, of the lateral displacement demand and of the residual deformations.

Analytical formulations are derived in order to evaluate the lateral stiffness and internal actions of precast hinged portal-frame with such additional devices. The derived formulations allow the selection of the device activation load, i.e. friction for ED device and pre-tension for SR device, that should occur before yielding of the column base. A design procedure is developed and applied to a selected case study resembling a precast portal frame of single-storey industrial buildings. The procedure is validated by means of non-linear time history analyses. The results show a general reduction of the column cross-section dimensions and of the amount of longitudinal rebars when the additional devices are considered. The use of SR devices, with or without ED, led to almost zero residual displacements, although the load in the beam-to-column connection almost doubled.

Even though the paper considered the performance in the transverse direction of portal frame structures, additional devices could be applied also in the longitudinal direction as between columns and gutter beams or between adjacent precast cladding panels.

Acknowledgements

Part of the work was financed by the Italian Civil Protection Department (Executive Project 2009-2012 Line E1: “Advanced seismic protection techniques for precast concrete structures”). Such financial support is gratefully acknowledged. The authors express their gratitude to Eng. S. Burini and Eng. D. Chiarini who were partially involved in the research during their undergraduate studies. The contribution of Eng. G. Fagà in drafting Figure 1b is greatly acknowledged. The opinions, findings, and conclusions expressed in the paper are those of the authors, and do not necessarily reflect the views of other individuals and organizations acknowledged.

References

[1] Psycharis IN, Mouzakis HP (2012): Shear resistance of pinned connections of precast members to monotonic and cyclic loading. Engineering Structures, 41, 413–427.

[2] Magliulo G, Ercolino M, Cimmino M, Capozzi V, Manfredi G (2014): FEM analysis of the strength of RC beam-to-column dowel connections under monotonic actions. Construction and Building Materials, 69, 271–284.

[3] Zoubek B, Fischinger M, Isakovic T (2015): Estimation of the cyclic capacity of beam-to-column dowel connections in precast industrial buildings. Bulleting of Earthquake Engineering, 13, 2145–2168.

[4] Fernandes RM, El Debs MK, de Boria K, El Debs AL (2009): Behavior of Socket Base Connections Emphasizing Pedestal Walls. ACI Structural Journal, 106 (3), 268–278.

[5] Belleri A, Riva P (2012): Seismic performance and retrofit of precast concrete grouted sleeve connections. PCI journal, 57 (1), 97–109.

[6] Haber ZB, Saiidi MS, Sanders DH (2014): Seismic Performance of Precast Columns with Mechanically Spliced Column-Footing Connections. ACI Structural Journal, 111 (3), 639- 650.

[7] Metelli G, Beschi C, Riva P (2011): Cyclic behaviour of a column to foundation joint for concrete precast structures, European Journal of Environmental and Civil Engineering, 15(9):1297-1318

[8] Belleri A, Brunesi E, Nascimbene R, Pagani M, Riva P (2015): Seismic performance of precast industrial facilities following major earthquakes in the Italian territory. Journal of Performance of Constructed Facilities, 29 (5), 04014135.

[9] Magliulo G, Ercolino M, Petrone C, Coppola O, Manfredi G (2014): The Emilia earthquake: seismic performance of precast reinforced concrete buildings. Earthquake Spectra, 30 (2), 891–912.

[10] Bournas DA, Negro P, Taucer FF (2014): Performance of industrial buildings during the Emilia earthquakes in Northern Italy and recommendations for their strengthening. Bull. Earthquake Eng., 12(5), 2383–2404.

[11] Belleri A, Torquati M, Riva P, Nascimbene R (2015): Vulnerability assessment and retrofit solutions of precast industrial structures. Earthquakes and Structures, 8 (3), 801–820.

[12] Magliulo G, Ercolino M, Manfredi G (2016): Failure of a precast RC building due to Emilia-Romagna earthquakes. Engineering Structures, 118, 262–273

[13] Babic A, Dolsek M (2016): Seismic fragility functions of industrial precast building classes. Engineering Structures, 118, 357–370.

[14] Casotto C, Silva V, Crowley H, Nascimbene R, Pinho R (2015): Seismic fragility of Italian RC precast industrial structures. Engineering Structures, 94, 122–136.

[15] Belleri A, Torquati M, Marini A, Riva P (2016): Horizontal cladding panels: in-plane seismic performance in precast concrete buildings. Bulletin of Earthquake Engineering, 14 (4), 1103-1129.

[16] Scotta R, De Stefani L, Vitaliani R (2015): Passive control of precast building response using cladding panels as dissipative shear walls. Bulletin of Earthquake Engineering, 13 (11), 3527- 3552.

[17] Zoubek B, Isakovic T, Fischinger M (2016): Cyclic response of hammer-head strap cladding-to-structure connections used in RC precast building. Engineering Structures, 119, 135–148.

[18] Brunesi E, Nascimbene R, Bolognini D, Bellotti D (2015): Experimental investigation of the cyclic response of reinforced precast concrete framed structures. PCI Journal, 60, 57–79.

[19] Belleri A, Torquati M, Riva P (2014): Seismic performance of ductile connections between precast beams and roof elements. Magazine of Concrete Research, 66 (11), 553–562.

[20] Restrepo JI, Park R, Buchanan AH, (1995): Design of Connections of Earthquake Resisting Precast Reinforced Concrete Perimeter Frames. PCI Journal, 40 (5), 68-80.

[21] Negro, P., Bournas, D.A., and Molina F.J., (2013), "Pseudodynamic Tests on a Full-Scale 3-Storey Precast Concrete Building: Global Response", Elsevier Engineering Structures, 57, 594-608.

[22] Bournas, D.A., Negro P., and Molina F.J., (2013), "Pseudodynamic Tests on a Full-Scale 3-Storey Precast Concrete Building: Behavior of the Mechanical Connections and Floor Diaphragms", Elsevier Engineering Structures, 57, 609-627.

[23] Martinez Rueda JE (2002): On the evolution of energy dissipation devices for seismic design. Earthquake Spectra, 18 (2), 309-46.

[24] Martinelli P, Mulas G (2010): An innovative passive control technique for industrial precast frames. Engineering Structures, 32, 1123-1132.

[25] Dal Lago B, Biondini F, Toniolo G (2017): Experimental Investigation on Steel W-Shaped Folded Plate Dissipative Connectors for Horizontal Precast Concrete Cladding Panels. Journal of Earthquake Engineering, doi: 10.1080/13632469.2016.1264333

[26] Jacobsen LS (1960): Damping in Composite Structures. Proceedings of the Second World Conference on Earthquake Engineering, 1029-1044.

[27] Engineers Edge, "Coefficient of Friction Equation and Table Chart". Retrieved May 4, 2017, from http://www.engineersedge.com/coeffients_of_friction.htm

[28] CEN (2005), EN 1993-1:2005, Eurocode 3: Design of steel structures - Part 1-1: General rules and rules for buildings, European Committee for Standardization, Brussels, Belgium.

[29] Plumier A editor (2007): Guidelines for Seismic Vulnerability Reduction in the Urban Environment. LESSLOSS Report - 2007/04. IUSS press, Pavia, Italy,

[30] D.M. 14/01/2008, Italian Building Code (2008) - Norme tecniche per le costruzioni. (in Italian).

[31] CEN (2004), EN 1998-1:2004, Eurocode 8: Design of structures for earthquake resistance - Part 1: General rules, seismic actions and rules for buildings, European Committee for Standardization, Brussels, Belgium.

[32] Venmarcke EH, Gasparini DA (1976): Simulated Earthquake Motions Compatible with Prescribed Response Spectra – SIMQKE-1. M.I.T. Department of Civil Engineering Research Report R76-4

[33] Ambraseys N, Smit P, Douglas J et al. (2004): Internet-site for European strong-motion data. Bollettino di Geofisica Teorica ed Applicata 45 (3), 113–129

[34] MidasGEN (2012) v3.1, MIDAS Information Technologies Co. Ltd

[35] Takeda T, Sozen MA, Nielsen NN (1970): Reinforced concrete response to simulated earthquakes. Journal of the Structural Division, 96 (12), 2557–2573.

[36] FEMA 356 (2000), Prestandard and commentary for the seismic rehabilitation of buildings. Federal Emergency Management Agency Washington, D.C.

[37] Priestley MJN, Calvi GM, Kowalsky MJ (2007): Displacement-Based Seismic Desgin of Structures. IUSS press, Pavia, Italy.

[38] Belleri A (2009): Displacement Based Design for Precast Concrete Structures. PhD tesi, University of Trento, Italy.

[39] Belleri A (2017): Displacement based design for precast concrete frames with not-emulative connections. Engineering Structures, 141, 228-240.